Supplementary Information for: Hyper-Auxeticity and the Volume Phase Transition of Polymer Gels

Andrea Ninarello[1,2,*] and Emanuela Zaccarelli[1,2,†]

[1] *CNR Institute of Complex Systems, Uos Sapienza, Piazzale Aldo Moro 2, 00185, Roma, Italy*
[2] *Department of Physics, Sapienza University of Rome, Piazzale Aldo Moro 2, 00185 Roma, Italy*

(Dated: May 28, 2025)

ADDITIONAL SIMULATION METHODS

We perform Molecular Dynamics simulations of polymer networks composed of monomers that interact through the Kremer-Grest potential. The excluded volume for all particles is described by the Weeks–Chandler–Andersen (WCA) potential [1]:

$$V_{WCA}(r) = 4\epsilon\left[\left(\frac{\sigma}{r}\right)^{12} - \left(\frac{\sigma}{r}\right)^{6}\right] + \epsilon \quad \text{if} \quad r \leq 2^{1/6}\sigma, \tag{S1}$$

where σ is the monomer diameter, which sets the unit of length, and ϵ controls the energy scale. Defining m as the mass of the particles, the unit time of our simulations is defined as $\tau = \sqrt{m\sigma^2/\epsilon}$. Chemical bonds between connected monomers are modeled by a FENE potential $V_{FENE}(r)$ [2]:

$$V_{FENE}(r) = -\epsilon k_F R_0^2 \ln\left[1 - \left(\frac{r}{R_0\sigma}\right)\right] \quad \text{if} \quad r < R_0\sigma, \tag{S2}$$

where $k_F = 15$ is the spring constant and $R_0 = 1.5$ is the maximum extension of the bond. To simulate the presence of the solvent and the polymer progressively going from a hydrophilic to a hydrophobic condition with increasing temperature, we employ a so-called solvophobic potential [3] of the form:

$$V_\alpha(r) = \begin{cases} -\epsilon\alpha & r \leq 2^{\frac{1}{6}}\sigma, \\ \frac{1}{2}\alpha\epsilon\big[\cos(\gamma(\frac{r}{\sigma})^2 + \beta) - 1\big] & 2^{\frac{1}{6}}\sigma < r < R_0\sigma, \end{cases} \tag{S3}$$

where $\gamma = (\pi(2.25 - 2^{1/3})^{-1})$, $\beta = 2\pi - 2.25\gamma$, ϵ is the unit of energy and the parameter α controls the strength of the monomer-monomer attractive interactions.

As anticipated in the main text, we employ networks with two different topologies. In one case, we build networks with an ordered structure based on a diamond-like lattice by crosslinking equal length chains where monomers are placed at the equilibrium distance of the FENE potential. The crosslinkers concentration is therefore directly determined by the chain length l through the relationship: $c = 1/(2l + 1)$. The total number of monomers N of the networks is $N = \frac{N_c}{c}$ where N_c is the number of crosslinkers. We employ systems as in Table S1.

c	l	N_c	N
0.5	99	64	12736
1	49	64	6336
2	25	64	3264
3	16	216	7128
5	10	216	4536
7.5	6	512	6656

TABLE S1. Table with crosslinker concentration, strand length, number of crosslinks, and total number of monomers for the ordered systems.

* andrea.ninarello@cnr.it

† emanuela.zaccarelli@cnr.it

In the disordered case, we considered a network with $N = 4384$ total number of monomers, of which $N_c = 49$ crosslinkers. This system is assembled through a recently developed technique [4, 5], which makes us able to produce low density computational polymer networks. In this method, one introduces patchy particles into a box with periodic boundary conditions; these particles are repulsive, each featuring either two or four attractive patches arranged tetrahedrally or positioned at the poles to represent crosslinkers and monomers, respectively indicated in the following as A and B patches. The interaction potential between particles i and j is defined as follows:

$$V(\mathbf{r}_{ij}, \mathbf{p}_i, \mathbf{p}_j) = V_{WCA}(r_{ij}) + \sum_{\mu \in \mathbf{p}_i} \sum_{\nu \in \mathbf{p}_j} V_{patchy}(r_{\mu\nu}) \tag{S4}$$

where the first addend indicates the presence of a WCA repulsion as introduced in Eq. S1 while the second addend is a sum over patches (μ, ν) belonging to the two particles whose positions are identified by a unit vector $\mathbf{p}_i^\mu, \mathbf{p}_j^\nu$. The V_{patchy} potential reads:

$$V_{patchy}(r_{\mu\nu}) = 2\epsilon_{\mu\nu} \left(\frac{\sigma_p^4}{2r_{\mu\nu}^4 - 1} \right) \exp\left(\frac{\sigma_p}{r_{\mu\nu} - r_c} + 2 \right) \quad \text{if} \quad r_{\mu\nu} \leq r_c \tag{S5}$$

where $\sigma_p = 0.4$ indicates the position of an attractive well of depth $\epsilon_{\mu\nu}$ and $r_c = 1.5\sigma_p$ is chosen by imposing $V_{patchy}(r_c) = 0$. We also set $\epsilon_{AB} = \epsilon_{BB} = \epsilon$ and $\epsilon_{AA} = 0$, so that we only allow bonding between the BB and AB patches. Additionally, we incorporate a three-body potential that acts on triplets of nearby patches, following the method in Ref. [6]. This approach enables an efficient bond-swapping mechanism that rapidly equilibrates the system at very low temperatures while maintaining the single-bond-per-patch constraint.

The assembly is performed via NVT molecular dynamics simulations at low temperature $T = 0.3$ and density $\rho = 2.85 \times 10^{-2}$ with the OxDNA package [7, 8]. We wait until the 99.9% of possible bonds are satisfied, then we remove all particles that do not belong to the largest cluster and all dangling chains in order to have a fully connected network without defects. This choice allows us to gain better control over the network's properties, as we observed in studies of both phantom and fully volume-excluded disordered systems (see Refs. [5, 9]). Dangling chains indeed tend to distort the system's statistical properties, as they typically do not contribute to elasticity. Once the assembly is ready, we then substitute the patchy reversible bonds with the bead-spring model.

BULK AND YOUNG MODULI

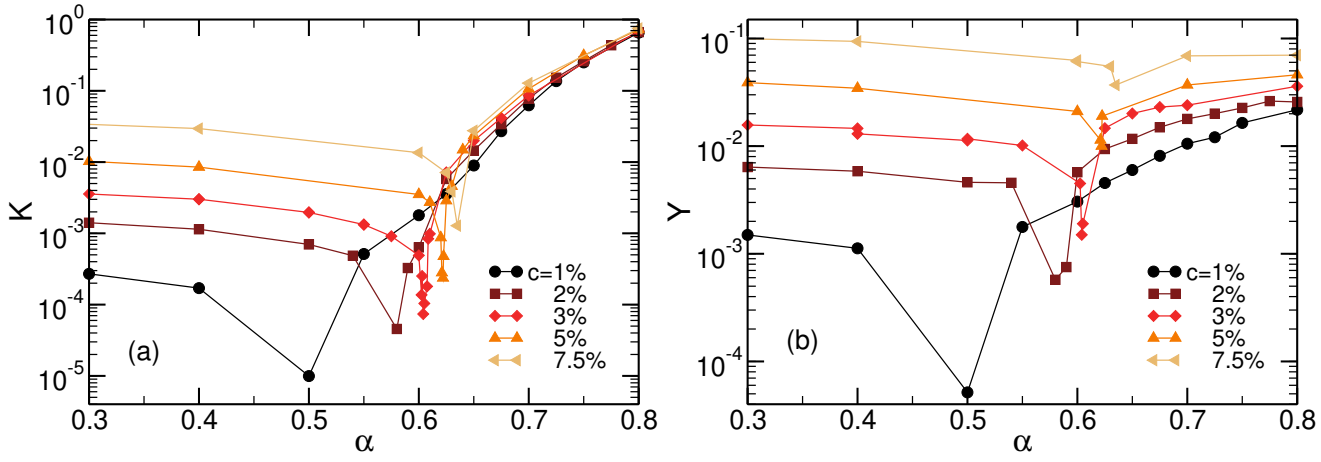

FIG. S1. Bulk (a) and Young (b) moduli as a function of α for $c = 1, 2, 3, 5, 7.5\%$ and corresponding $P = 9.25 \times 10^{-4}, 3.5 \times 10^{-3}, 7.9 \times 10^{-3}, 1.8 \times 10^{-2}, 4.25 \times 10^{-2}$.

As discussed in the main text, the behavior of the bulk K modulus for our hydrogels suggests the presence of an underlying criticality. In particular, a vanishing bulk modulus is related with the presence of critical-like fluctuations of the system volume, hinting at the occurrence of a second order transition as observed for instance in martensitic transformations [10]. In Fig. S1(a) we report the bulk modulus as a function of α for different c values, corresponding to the state points shown in Fig.3(a) of the main text. At low α, the elasticity of the network is strongly influenced by

c, with K spanning up to two orders of magnitude as c increases. However, increasing α, K shows a dramatic decrease with a minimum reaching very low values as c decreases, up to about five orders of magnitude with respect to the high compact state observed at large α when all networks behave in the same way. We report the corresponding behavior of the Young modulus Y in Fig. S1(b). Although Y is not expected to show critical behavior, we observe the same qualitative trend also present in K, with a clear minimum also developing, becoming more and more pronounced as c decreases. Beyond the VPT, Y increases with α, but unlike K, it remains clearly separated for different values of c.

DISORDERED EQUATION OF STATE

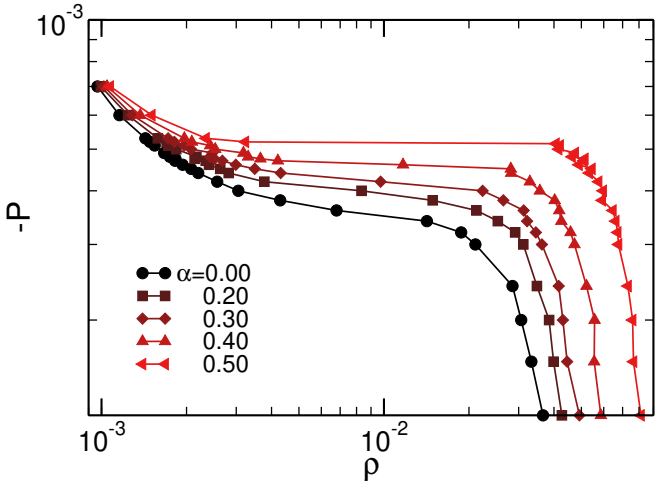

FIG. S2. Pressure versus density of the $c = 1\%$ disordered system for different values of α

The equation of state for the disordered system at various values of α is reported in Fig. S2 for the sake of completeness. As can be observed, the results are largely consistent with those of the ordered system, though the transition occurs at a slightly lower α than in the ordered case. This earlier transition in the disordered system was also noted in Ref. [11], although in that study the driving parameter for the transition, which decreased in absolute value, was the pressure. This behavior can be attributed to density inhomogeneities, which make the disordered structure more easily stretched.

SIZE EFFECTS

To address the relevance of size scaling, we conducted additional simulations for a larger system at $c = 1\%$. The results are presented in Fig. S3. The left panel shows the swelling curve of the diamond network at $c = 1\%$ for two different system sizes, as specified in the legend. The two curves, when appropriately rescaled by the volume at $\alpha = 0$, perfectly align, demonstrating consistency between scales. However, due to computational limitations, the larger system was analyzed at fewer state points.

Building on this result, we further explored the properties of the larger system near the transition, both in equilibrium and under uniaxial deformation. In particular, we observed the same critical fluctuations discussed in the main manuscript for the smaller system, as depicted in the right panel of Fig. S3. Moreover, strain-stress simulations at this state point revealed an elastic response with a Poisson's ratio of $\nu \approx -0.9$, indicating behavior very close to the hyper-auxetic condition.

These preliminary findings reinforce the conclusions presented in the manuscript. Nonetheless, they highlight the need for more comprehensive investigations of size scaling, which will be pursued in future work.

PHASE SEPARATION OF POLYMER CHAINS

To allow comparison with network results, we also explore chain-based systems of different lengths l. We therefore perform MD simulations of chains of equal length $l = 1, 2, 5, 10, 49, 156, 500$, varying the total number of all monomers

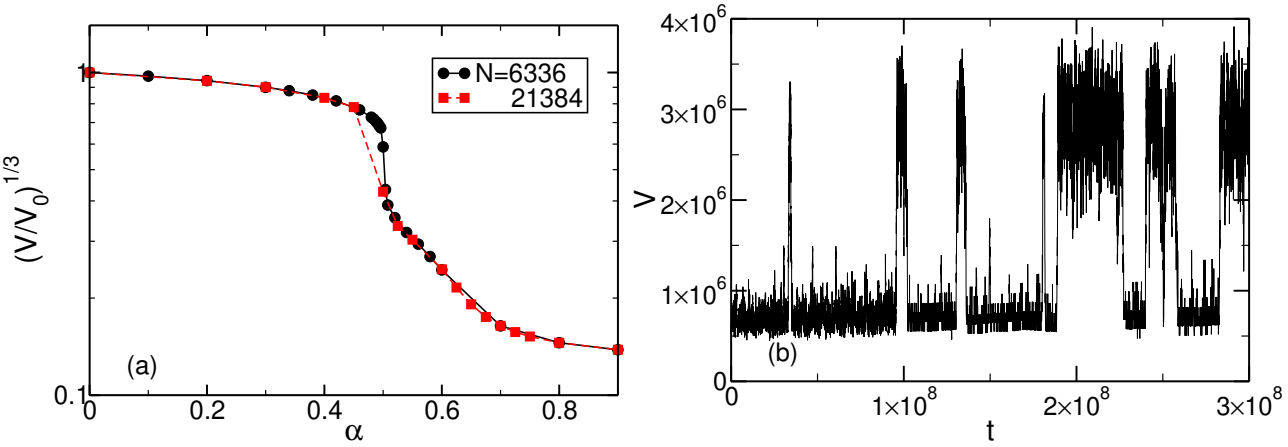

FIG. S3. (a) Swelling curve for two system sizes as indicated in the legend for the $c = 1\%$ system. (b) Volume as a function of time for the $N = 21384$, $c = 1\%$ system at $\alpha = 0.502$. All results are obtained at $P = -9.25 \times 10^{-4}$.

in the range $n \in [10000, 20000]$.

To allow a quick scan of the phase diagram in order to look for phase separation, for each chain length we perform several NVT simulations at different attractive strengths α and system volume. After allowing the system to equilibrate for 2×10^6 time steps, we generate multiple equilibrium configurations by running simulations for 10^7 time steps. These configurations are used to calculate the structure factor $S(k)$ of the network, which is computed removing the (almost negligible) contribution of the single chain form factor $S_1(k)$. Here, k is the modulus of the wave vector. Subsequently, we extract the value at $S(k)$ at the smallest simulated value of k, namely, $k_{min} = \frac{2\pi}{L}$, with L representing the box side. In this way, we have access to a proxy for the isothermal compressibility κ_T of the system (that is, the inverse of the bulk modulus for network systems), since $S(k \to 0)$ is directly related to the system through equation $\kappa_T = \frac{S(0)}{\rho K_B T}$ [12]. It is important to note that κ_T theoretically approaches infinity at phase separation in infinite-size systems, but for finite systems, density fluctuations remain finite, although showing a significant growth.

We report $S(k_{min})/S_1(k_{min})$ as a function of α for several isochores studied for the $l = 49$ system in Fig. S4(a) as a representative example of our analysis. Increasing α, a clear increase in $S(k_{min})$ is observed, which passes through an inflection point at a decreasing value of α with increasing volume. At large volumes, the behavior saturates, collapsing onto the same curve, with a value of $S(k_{min})/S_1(k_{min})$ jumping by more than two orders of magnitude for a slight increase of α. We identify this inflection point with the critical value α_c that is required to induce phase separation. As we aim to compare these results with the network system ones, it is particularly relevant to perform a similar analysis with varying the chain length. This is reported in Fig. S4(b) where we report $S(k_{min})/S_1(k_{min})$ for each studied l at the volume where the phase-separation temperature α_c is smallest. Therefore, we observe a clear decrease of α_c with increasing l, approaching the value of the VPT ($\alpha_{VPT} \sim 0.65$) for $l > 100$, as shown in the main text in Fig. 3(b). Since networks generally contain predominantly longer chains that dominate the phase behavior, we conclude that the volume phase transition (VPT) arises purely from the solvophobic attraction between monomers as α increases. The universal value α_{VPT} reflects the dominant role of long chains in both hydrogels and microgels.

[1] J. D. Weeks, D. Chandler, and H. C. Andersen, Role of repulsive forces in determining the equilibrium structure of simple liquids, The Journal of Chemical Physics **54**, 5237–5247 (1971).

[2] K. Kremer and G. S. Grest, Dynamics of entangled linear polymer melts: A molecular-dynamics simulation, The Journal of Chemical Physics **92**, 5057–5086 (1990).

[3] T. Soddemann, B. Dünweg, and K. Kremer, The European Physical Journal E **6**, 409–419 (2001).

[4] N. Gnan, L. Rovigatti, M. Bergman, and E. Zaccarelli, In silico synthesis of microgel particles, Macromolecules **50**, 8777–8786 (2017).

[5] V. Sorichetti, V. Hugouvieux, and W. Kob, Dynamics of nanoparticles in polydisperse polymer networks: from free diffusion to hopping, Macromolecules **54**, 8575–8589 (2021).

[6] F. Sciortino, Three-body potential for simulating bond swaps in molecular dynamics, The European Physical Journal E **40**, 10.1140/epje/i2017-11496-5 (2017).

[7] L. Rovigatti, P. Šulc, I. Z. Reguly, and F. Romano, A comparison between parallelization approaches in molecular dynamics simulations on gpus, Journal of Computational Chemistry **36**, 1–8 (2014).

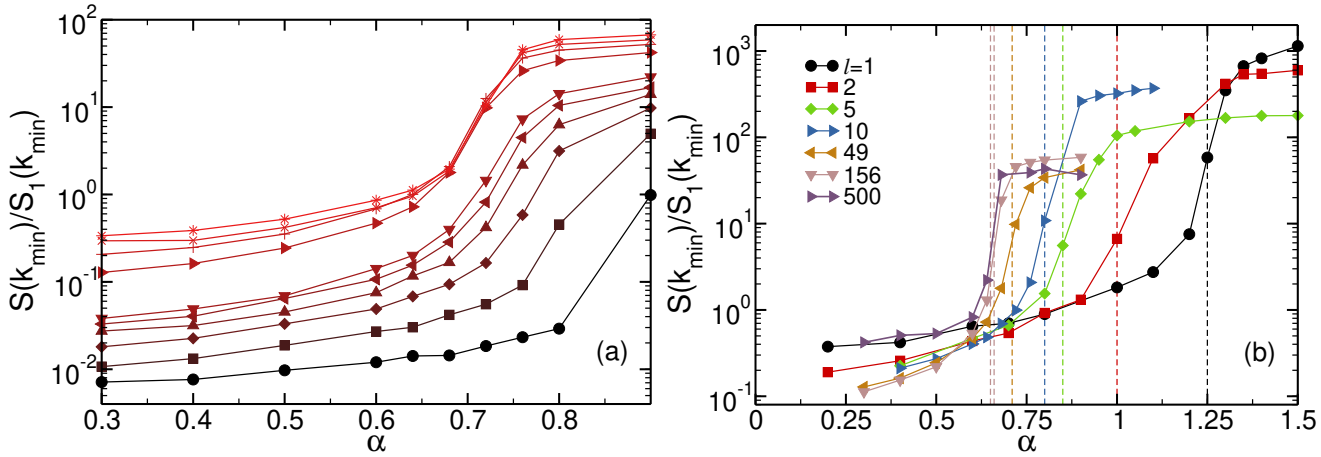

FIG. S4. Value of the structure factor at the minimum accessible wave vector $S(k_{min})$ as a function of α, rescaled by the single chain form factor at the same point $S_1(k_{min})$. (a) Results for the $l = 49$ system for different volumes increasing from bottom to top in the interval $V = 1 \times 10^3 - 1 \times 10^4$. (b) Results for systems with various chain lengths as indicated in the legend at the volume corresponding to the steepest variation. Vertical lines highlight the inflection points that identify the transition temperature α_c for each l.

[8] E. Poppleton, J. Bohlin, M. Matthies, S. Sharma, F. Zhang, and P. Šulc, Design, optimization and analysis of large dna and rna nanostructures through interactive visualization, editing and molecular simulation, Nucleic Acids Research **48**, e72–e72 (2020).

[9] V. Sorichetti, A. Ninarello, J. Ruiz-Franco, V. Hugouvieux, E. Zaccarelli, C. Micheletti, W. Kob, and L. Rovigatti, Structure and elasticity of model disordered, polydisperse, and defect-free polymer networks, The Journal of Chemical Physics **158**, 10.1063/5.0134271 (2023).

[10] L. Dong, D. S. Stone, and R. S. Lakes, Softening of bulk modulus and negative poisson ratio in barium titanate ceramic near the curie point, Philosophical Magazine Letters **90**, 23–33 (2010).

[11] A. Ninarello, J. Ruiz-Franco, and E. Zaccarelli, Auxetic polymer networks: The role of crosslinking, density, and disorder, The Journal of Chemical Physics **159**, 10.1063/5.0178409 (2023).

[12] J.-P. Hansen and I. R. McDonald, Introduction, in *Theory of Simple Liquids* (Elsevier, 2013).